THE PROFILES OF FRAUNHOFER LINES IN THE PRESENCE OF ZEEMAN SPLITTING

I: *The Zeeman Triplet*

J. M. BECKERS

Sacramento Peak Observatory, Air Force Cambridge Research Laboratories, Sunspot, N.M., U.S.A.

(Received 8 April, 1969)

Abstract. For the case of pure absorption lines (LTE) a method is described which enables the general computation of Zeeman-split line profiles. The magnetic field vector, the Doppler shift and the line absorption coefficient is permitted to vary arbitrarily with optical depth. Elliptical birefringence (e.g., Faraday rotation) of the solar atmosphere is taken into account. Some numerical examples are given and some interesting behaviors of the line profiles are discussed.

1. Introduction

A number of papers have been devoted to the formation of Fraunhofer lines. Moe (1968) summarizes these. All these papers make some assumptions. Moe's theory is so far the most complete one for lines formed in local thermodynamics equilibrium (LTE). However, it cannot treat cases in which the magnetic field varies with depth or in which a velocity field is associated with the magnetic structure of the solar atmosphere.

This paper gives the results of a direct numerical evaluation of the transfer equations. It can take into account any model atmosphere, any variation of the line absorption coefficient with depth and any variation of the magnetic and velocity field with depth. The only restriction is LTE.

2. The Transfer Equations

This paper uses the same notation as Moe (1968). The angle of the magnetic vector to the line of sight will be $\gamma(\tau)$, the azimuth with respect to an arbitrary X-axis (at right angles to the line of sight) will be $\chi(\tau)$, and the scalar value of the field will be $\mathrm{H}(\tau)$. Since variations of the field azimuth will be considered, one has to use all the four Stokes parameters I, Q, U and V.

The Unno (1956) transfer equations then change to:

$$\cos\theta \frac{\mathrm{d}I}{\mathrm{d}\tau} = (1 + \eta_I)(I - B) + \eta_Q Q + \eta_U U + \eta_V V \tag{1}$$

$$\cos\theta \frac{\mathrm{d}Q}{\mathrm{d}\tau} = (1 + \eta_I) Q + \eta_Q (I - B) \tag{1'}$$

$$\cos\theta \frac{\mathrm{d}U}{\mathrm{d}\tau} = (1 + \eta_I) U + \eta_U (I - B) \tag{1''}$$

$$\cos\theta \frac{\mathrm{d}V}{\mathrm{d}\tau} = (1 + \eta_I) V + \eta_V (I - B) \tag{1'''}$$

Solar Physics **9** (1969) 372–386; © *D. Reidel Publishing Company, Dordrecht-Holland*

where

$$\eta_I = \frac{\eta_p}{2}\sin^2\gamma + \frac{\eta_b + \eta_r}{4}(1 + \cos^2\gamma) \tag{2}$$

$$\eta_Q = \left(\frac{\eta_p}{2} - \frac{\eta_b + \eta_r}{4}\right)\sin^2\gamma\cos 2\chi \tag{2'}$$

$$\eta_U = \left(\frac{\eta_p}{2} - \frac{\eta_b + \eta_r}{4}\right)\sin^2\gamma\sin 2\chi \tag{2''}$$

$$\eta_V = \frac{\eta_b - \eta_r}{2}\cos\gamma \tag{2'''}$$

where η_p, η_b and η_r are the line absorption coefficients centered at the π and at the blue and red elliptically polarized σ components with respect to the continuum absorption coefficient.

The Equations (1) are a simple set of first order differential equations which can be numerically integrated step by step using only boundary values for I, Q, U and V for a large value of τ.

Reasonably good boundary values are: $I_B = B(\tau_B)$, $Q_B = U_B = V_B = 0$ where τ_B is the boundary τ. Better boundary values are:

$$I_B = B + [B'\cos\theta(1 + \eta_I)]/[(1 + \eta_I)^2 - \eta_Q^2 - \eta_U^2 - \eta_V^2] \tag{3}$$

$$Q_B = -B'\cos\theta\eta_Q/[(1 + \eta_I)^2 - \eta_Q^2 - \eta_U^2 - \eta_V^2] \tag{3'}$$

$$U_B = -B'\cos\theta\eta_U/[(1 + \eta_I)^2 - \eta_Q^2 - \eta_U^2 - \eta_V^2] \tag{3''}$$

$$V_B = -B'\cos\theta\eta_V/[(1 + \eta_I)^2 - \eta_Q^2 - \eta_U^2 - \eta_V^2] \tag{3'''}$$

where η, B and $B' \equiv \mathrm{d}B/\mathrm{d}\tau$ are taken at τ_B. These boundary values are the exact solutions for a Milne-Eddington-type atmosphere with $B = B_0(1 + \beta_0\tau)$ and $\eta = \eta\ (\tau_B)$.

The solution of the set of differential Equations (1) was done by means of a Runge-Kutta technique (see, e.g., Abramowitz and Stegun, page 896).

3. The Faraday and the Voigt Effects

Apart from the change of absorption coefficient near the position of a Fraunhofer line, there is also a change of the refractive index and the speed of light. For solar conditions this change in refractive index is extremely small which is why theories using the anomalous dispersion or refraction to explain various solar phenomena (e.g., Julius, 1928) were rather unsuccessful.

When the line shows a Zeeman splitting, the change in refractive index at any one wavelength near the line becomes different for the different polarizations. For a longitudinal magnetic field this difference is between left- and right-hand circular polarization and the resulting circular birefringence gives the so-called Faraday

rotation or Macaluso-Corbino effect. This rotation per cm is small but, because of the long depth in the solar atmosphere over which lines are formed, the resulting rotation may be significant (Severny, 1959; Kai, 1968; Rachkovsky, 1962a, b). For a longitudinal magnetic field the polarization of the Zeeman triplet components is circular so that the Faraday rotation is of no interest. However, in case of a magnetic field with a variable direction, as considered in this paper, the Faraday rotation has to be considered. In case of a transverse field the refractive index differences result in linear birefringence and the so-called Voigt effect occurs (see, e.g., Born, 1965, page 508). For an arbitrary direction of the magnetic field, one has elliptical birefringence* of the solar atmosphere.

The refractive index near an absorption line, in absence of Doppler broadening, varies as follows:

$$(n-1) = \frac{e^2}{4\pi mc^2} Nf \frac{\Delta\lambda \cdot \lambda^3}{(\Delta\lambda)^2 + \left(\frac{\Gamma\lambda^2}{4\pi c}\right)^2} \tag{4}$$

where N equals the number of atoms per cm^3 involved in the absorption and Γ is the damping constant. It is useful to compare this with the absorption coefficient at line center κ_0

$$\kappa_0 = \frac{\sqrt{\pi}e^2}{mc^2} Nf \frac{\lambda^2}{\Delta\lambda_D} H(0, a) \tag{5}$$

where the Voigt profile $H(\Delta\lambda/\Delta\lambda_D, a)$ equals $\sum_{n=0}^{4} a^n H_n(\Delta\lambda/\Delta\lambda_D)$ with the H_n listed by Aller (1963, Table 7-1). From (5) Equation (4) becomes:

$$(n-1) = \frac{\kappa_0\lambda}{4\pi^{3/2}H(0, a)} \frac{v}{v^2 + a^2} \quad \text{with} \quad v \equiv \frac{\Delta\lambda}{\Delta\lambda_D} \quad \text{and} \quad a = \frac{\Gamma\lambda^2}{4\pi c\Delta\lambda_D}. \tag{6}$$

We now estimate the significance of this effect in the solar atmosphere. Since a is small and $V(0, a) \approx 1$, Equation (6) gives for $v = 1$ $(n-1) = \kappa_0\lambda/4\pi^{3/2}$. For Zeeman splittings large compared to $\Delta\lambda_D$, the retardation of the solar atmosphere down to depth D equals:

$$\int_0^D \frac{(n-1)}{\lambda} \, dx = (4\pi^{3/2})^{-1} \, t_0, \quad \text{where} \quad t_0 \equiv \int_0^D \kappa_0 \, dx. \tag{7}$$

For $t_0 = 1$ Equation (7) gives 0.045 orders retardation which is large enough to be of significance. The retardation will be larger for smaller v and larger t_0. Very little radiation emerges when t_0 is larger. Hence, no large increase can be expected there. Decreasing v also gives little increase if the Doppler broadening is included in Equa-

* From now on I shall imply the general elliptical case when talking about birefringence and retardation.

tion (6). According to Born (1965, page 482) Doppler broadening changes (6) into:

$$(n-1) = \frac{\kappa_0 \lambda}{4\pi^2 H(0,a)} \int_{-\infty}^{+\infty} \frac{u}{u^2+a^2} e^{-(u-v)^2} du \tag{8}$$

$$= \frac{\kappa_0 \lambda}{4\pi a H(0,a)} \left[\frac{1}{2} \frac{dH(v,a)}{dv} + v \cdot H(v,a) \right] \tag{8'}$$

$$\equiv \frac{\kappa_0 \lambda}{2\pi H(0,a)} F(v,a). \tag{8''}$$

The function $F(v, a)$ can be expressed in a power series of a of the form:

$$F(v,a) = \sum_{n=0}^{3} a^n F_i(v). \tag{9}$$

The functions F_i are given by Rachkovsky (1962a) and are tabulated in Table I.

TABLE I

The functions F_i as given by Rachkovsky

v	F_0	F_1	F_2	F_3
0.0	0.0000	0.0000	0.0000	0.0000
0.1	0.0560	−0.0990	0.1113	−0.0983
0.2	0.1099	−0.1922	0.2139	−0.1870
0.3	0.1595	−0.2742	0.3000	−0.2577
0.4	0.2031	−0.3409	0.3638	−0.3045
0.5	0.2395	−0.3894	0.4018	−0.3245
0.6	0.2679	−0.4186	0.4135	−0.3181
0.7	0.2880	−0.4288	0.4007	−0.2888
0.8	0.3002	−0.4218	0.3673	−0.2419
0.9	0.3051	−0.4004	0.3186	−0.1842
1.0	0.3036	−0.3679	0.2606	−0.1226
1.1	0.2969	−0.3280	0.1990	−0.0634
1.2	0.2862	−0.2843	0.1390	−0.0114
1.3	0.2727	−0.2399	0.0844	0.0304
1.4	0.2576	−0.1972	0.0378	0.0605
1.5	0.2416	−0.1581	0.0006	0.0790
1.6	0.2256	−0.1237	−0.0269	0.0874
1.7	0.2102	−0.0945	−0.0456	0.0876
1.8	0.1956	−0.0705	−0.0566	0.0818
1.9	0.1822	−0.0514	−0.0614	0.0723
2.0	0.1700	−0.0366	−0.0617	0.0611
2.1	0.1590	−0.0255	−0.0589	0.0495
2.2	0.1492	−0.0174	−0.0541	0.0387
2.3	0.1405	−0.0116	−0.0485	0.0293
2.4	0.1328	−0.0076	−0.0426	0.0215
2.5	0.1259	−0.0048	−0.0369	0.0153
2.6	0.1197	−0.0030	−0.0318	0.0106
2.7	0.1142	−0.0018	−0.0272	0.0071
2.8	0.1092	−0.0011	−0.0233	0.0047
2.9	0.1047	−0.0006	−0.0200	0.0030
3.0	0.1006	−0.0004	−0.0173	0.0019

Table I (continued)

v	F_0	F_1	F_2	F_3
3.1	0.0968	−0.0002	−0.0150	0.0011
3.2	0.0934	−0.0001	−0.0131	0.0007
3.3	0.0902	−0.0001	−0.0115	0.0004
3.4	0.0872	−0.0000	−0.0102	0.0002
3.5	0.0844	−0.0000	−0.0091	0.0001
3.6	0.0818	−0.0000	−0.0081	0.0001
3.7	0.0794	−0.0000	−0.0073	0.0000
3.8	0.0771	−0.0000	−0.0067	0.0000
3.9	0.0750	−0.0000	−0.0060	0.0000
4.0	0.0730	−0.0000	−0.0055	0.0000
4.1	0.0711	−0.0000	−0.0051	0.0000
4.2	0.0693	−0.0000	−0.0047	0.0000
4.3	0.0675	−0.0000	−0.0043	0.0000
4.4	0.0659	−0.0000	−0.0039	0.0000
4.5	0.0644	−0.0000	−0.0037	0.0000
4.6	0.0629	−0.0000	−0.0034	0.0000
4.7	0.0615	−0.0000	−0.0032	0.0000
4.8	0.0601	−0.0000	−0.0030	0.0000
4.9	0.0589	−0.0000	−0 0027	0 0000
5.0	0.0576	−0.0000	−0.0026	0.0000
5.1	0.0564	−0.0000	−0.0024	0.0000
5.2	0.0553	−0.0000	−0.0023	0.0000
5.3	0.0542	−0.0000	−0.0021	0.0000
5.4	0.0532	−0.0000	−0.0020	0.0000
5.5	0.0522	−0.0000	−0.0019	0.0000
5.6	0.0512	−0.0000	−0.0018	0.0000
5.7	0.0503	−0.0000	−0.0017	0.0000
5.8	0.0494	−0.0000	−0.0016	0.0000
5.9	0.0485	−0.0000	−0.0015	0.0000
6.0	0.0477	−0.0000	−0.0014	0.0000
6.1	0.0469	−0.0000	−0.0013	0.0000
6.2	0.0461	−0.0000	−0.0013	0.0000
6.3	0.0454	−0.0000	−0.0012	0.0000
6.4	0.0446	−0.0000	−0.0012	0.0000
6.5	0.0439	−0.0000	−0.0011	0.0000
6.6	0.0432	−0.0000	−0.0010	0.0000
6.7	0.0426	−0.0000	−0.0010	0.0000
6.8	0.0419	−0.0000	−0.0010	0.0000
6.9	0.0413	−0.0000	−0.0009	0.0000
7.0	0.0407	−0.0000	−0.0009	0.0000
7.1	0.0401	−0.0000	−0.0008	0.0000
7.2	0.0396	−0.0000	−0.0008	0.0000
7.3	0.0390	−0.0000	−0.0008	0.0000
7.4	0.0385	−0.0000	−0.0008	0.0000
7.5	0.0380	−0.0000	−0.0007	0.0000
7.6	0.0374	−0.0000	−0.0007	0.0000
7.7	0.0370	−0.0000	−0.0007	0.0000
7.8	0.0365	−0.0000	−0.0006	0.0000
7.9	0.0360	−0.0000	−0.0006	0.0000
8.0	0.0355	−0.0000	−0.0006	0.0000
8.1	0.0351	−0.0000	−0.0005	0.0000
8.2	0.0347	−0.0000	−0.0005	0.0000
8.3	0.0342	−0.0000	−0.0005	0.0000

Table I (continued)

v	F_0	F_1	F_2	F_3
8.4	0.0338	−0.0000	−0.0005	0.0000
8.5	0.0334	−0.0000	−0.0005	0.0000
8.6	0.0330	−0.0000	−0.0005	0.0000
8.7	0.0326	−0.0000	−0.0005	0.0000
8.8	0.0323	−0.0000	−0.0004	0.0000
8.9	0.0319	−0.0000	−0.0004	0.0000
9.0	0.0315	−0.0000	−0.0004	0.0000
9.1	0.0312	−0.0000	−0.0004	0.0000
9.2	0.0308	−0.0000	−0.0004	0.0000
9.3	0.0305	−0.0000	−0.0004	0.0000
9.4	0.0302	−0.0000	−0.0004	0.0000
9.5	0.0299	−0.0000	−0.0004	0.0000
9.6	0.0295	−0.0000	−0.0004	0.0000
9.7	0.0292	−0.0000	−0.0003	0.0000
9.8	0.0289	−0.0000	−0.0003	0.0000
9.9	0.0286	−0.0000	−0.0003	0.0000
10.0	0.0284	−0.0000	−0.0003	0.0000
10.1	0.0281	−0.0000	−0.0003	0.0000
10.2	0.0278	−0.0000	−0.0003	0.0000
10.3	0.0275	−0.0000	−0.0003	0.0000
10.4	0.0273	−0.0000	−0.0003	0.0000
10.5	0.0270	−0.0000	−0.0002	0.0000
10.6	0.0267	−0.0000	−0.0002	0.0000
10.7	0.0265	−0.0000	−0.0002	0.0000
10.8	0.0262	−0.0000	−0.0002	0.0000
10.9	0.0260	−0.0000	−0.0002	0.0000
11.0	0.0258	−0.0000	−0.0002	0.0000
11.1	0.0255	−0.0000	−0.0002	0.0000
11.2	0.0253	−0.0000	−0.0002	0.0000
11.3	0.0251	−0.0000	−0.0002	0.0000
11.4	0.0248	−0.0000	−0.0002	0.0000
11.5	0.0246	−0.0000	−0.0002	0.0000
11.6	0.0244	−0.0000	−0.0002	0.0000
11.7	0.0242	−0.0000	−0.0002	0.0000
11.8	0.0240	−0.0000	−0.0002	0.0000
11.9	0.0238	−0.0000	−0.0002	0.0000
12.0	0.0236	−0.0000	−0.0001	0.0000
large v	$0.282\ v^{-1}$	0.0000	$-0.3\ v^{-3}$	0.000

$F(-v) = -F(v)$

For small a, Equation (9) gives a maximum for F at $v=0.93$ with $F_{\max}=0.31$. The total retardation for large Zeeman splitting at this maximum and for $t_0=1$ equals 0.05 orders. This is of the same magnitude as obtained by Rachkovsky. However, it is much smaller than suggested by Severny (1959) and Kai (1968).

The effect of this magnetic optical birefringence can easily be included in the transfer equations and their solution. It is easiest to think of each of the three components of the Zeeman triplet as being a separate elliptical retarder. The retardation $\mathrm{d}\varrho$ of a

layer of thickness dx for each of these components equals $2\pi\,\Delta n\,dx/\lambda$ radians which results in a retardation of three line components of:

$$dR_b = \frac{-\eta_0}{H(0,a)}\,\frac{(1+\cos^2\gamma)}{4}\,F(v+v_H,a)\,\frac{d\tau}{\cos\theta} \tag{10}$$

$$dR_p = \frac{-\eta_0}{H(0,a)}\,\frac{\sin^2\gamma}{2}\,F(v,a)\,\frac{d\tau}{\cos\theta} \tag{10'}$$

$$dR_r = \frac{-\eta_0}{H(0,a)}\,\frac{(1+\cos^2\gamma)}{4}\,F(v-v_H,a)\,\frac{d\tau}{\cos\theta}. \tag{10''}$$

The orientation of the axes of these elliptical retardations is indicated on the Poincaré sphere (Beckers, 1968) in Figure 1. The angle $\tilde{\gamma}$ is related to γ by $\tan\tilde{\gamma}=0.5\tan\gamma\,\sin\gamma$.

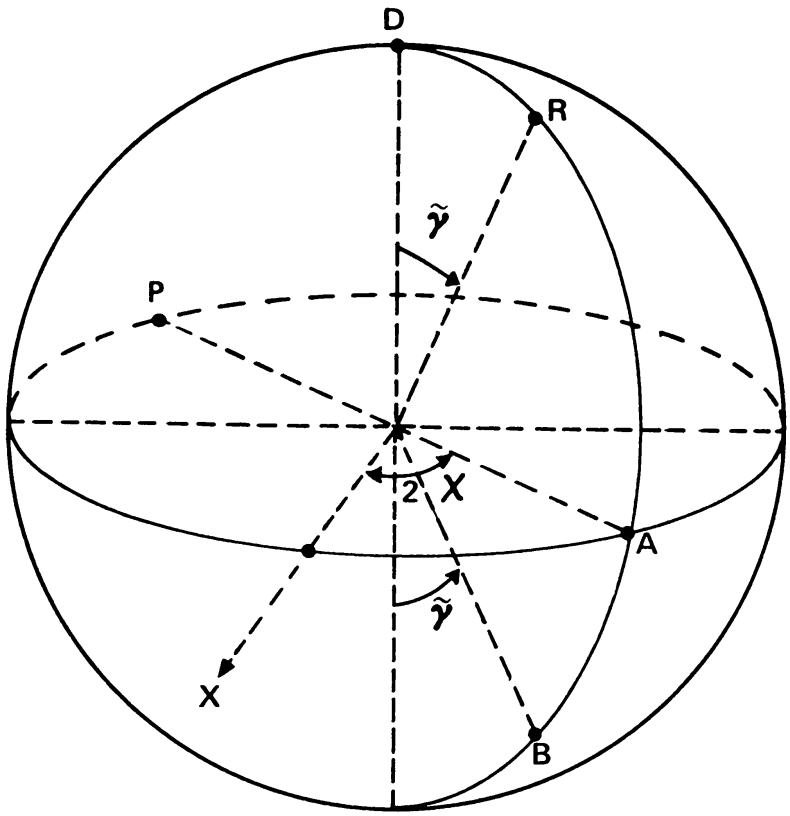

Fig. 1. The axis of birefringence of the blue and red σ components and of the π component are indicated by B, R and P on this Poincaré sphere. Their joint retardation can be represented by the combined action of a rotator (rotation of sphere around D) and a wave plate (rotation around A). The angles $\tilde{\gamma}$ and χ are defined in the text. X corresponds to the X-axis of the arbitrarily defined (X, Y) coordinate system with respect to which Q is measured.

The combined action of the three weak retarders can be represented by the action of a rotator (= circular retarder) equal to

$$(dR_r - dR_b)\cos\tilde{\gamma} \equiv -\varrho_R\,\frac{d\tau}{\cos\theta} \tag{11}$$

and by a wave plate (= linear retarder) with its optical axis parallel to the magnetic field azimuth and with a retardation equal to

$$(\mathrm{d}R_r + \mathrm{d}R_b)\sin\tilde{\gamma} - \mathrm{d}R_p \equiv -\varrho_W \frac{\mathrm{d}\tau}{\cos\theta}. \tag{12}$$

This gives for ϱ_R and ϱ_W the following expressions:

$$\varrho_R = \frac{\eta_0 \cos\tilde{\gamma}}{H(0,a)} \frac{(1+\cos^2\gamma)}{4} [F(v-v_H, a) - F(v+v_H, a)] \tag{13}$$

$$\varrho_W = \frac{\eta_0}{H(0,a)} \left\{ \frac{\sin\tilde{\gamma}(1+\cos^2\gamma)}{4} [F(v-v_H, a) + F(v+v_H, a)] - \frac{\sin^2\gamma}{2} F(v,a) \right\}. \tag{14}$$

This rotator and wave plate affect the four Stokes parameters as follows (see Figure 2):

$$\Delta I = 0 \tag{15}$$

$$\cos\theta\, \Delta Q = (V\varrho_W \sin 2\chi - U\varrho_R)\,\mathrm{d}\tau \tag{15'}$$

$$\cos\theta\, \Delta U = (-V\varrho_W \cos 2\chi + Q\varrho_R)\,\mathrm{d}\tau \tag{15''}$$

$$\cos\theta\, \Delta V = (U\cos 2\chi - Q\sin 2\chi)\,\varrho_W\,\mathrm{d}\tau, \tag{15'''}$$

and the Equations (1) change into:

$$\cos\theta \frac{\mathrm{d}I}{\mathrm{d}\tau} = (1+\eta_I)(I-B) + \eta_Q Q + \eta_U U + \eta_V V \tag{16}$$

$$\cos\theta \frac{\mathrm{d}Q}{\mathrm{d}\tau} = (1+\eta_I) Q + \eta_Q (1-B) - \varrho_R U + \varrho_W V \sin 2\chi \tag{16'}$$

$$\cos\theta \frac{\mathrm{d}U}{\mathrm{d}\tau} = (1+\eta_I) U + \eta_U (I-B) + \varrho_R Q - \varrho_W V \cos 2\chi \tag{16''}$$

$$\cos\theta \frac{\mathrm{d}V}{\mathrm{d}\tau} = (1+\eta_I) V + \eta_V (I-B) - \varrho_W (Q\sin 2\chi - U\cos 2\chi). \tag{16'''}$$

For the Equations (16) the signs of the various quantities are defined as follows. V is the light intensity when viewed in counterclockwise circular polarization minus that viewed in clockwise circular polarization. If (X, Y, Z) is a cartesian coordinate system with the Z-axis pointing to the observer, the angle between the magnetic field vector and the Z-axis is γ. The field azimuth χ is measured counterclockwise from the X-axis (the Y-axis coincides with $\chi = 90°$). Q is positive for light polarized in the direction of the X-axis, U is positive for light polarized at azimuth $\chi = 45°$. When $\varrho_R\,\mathrm{d}\tau$ or $\varrho_W\,\mathrm{d}\tau$ are positive, the Poincaré sphere in Figures 1 and 2 is rotated in a clockwise direction. v_H is positive.

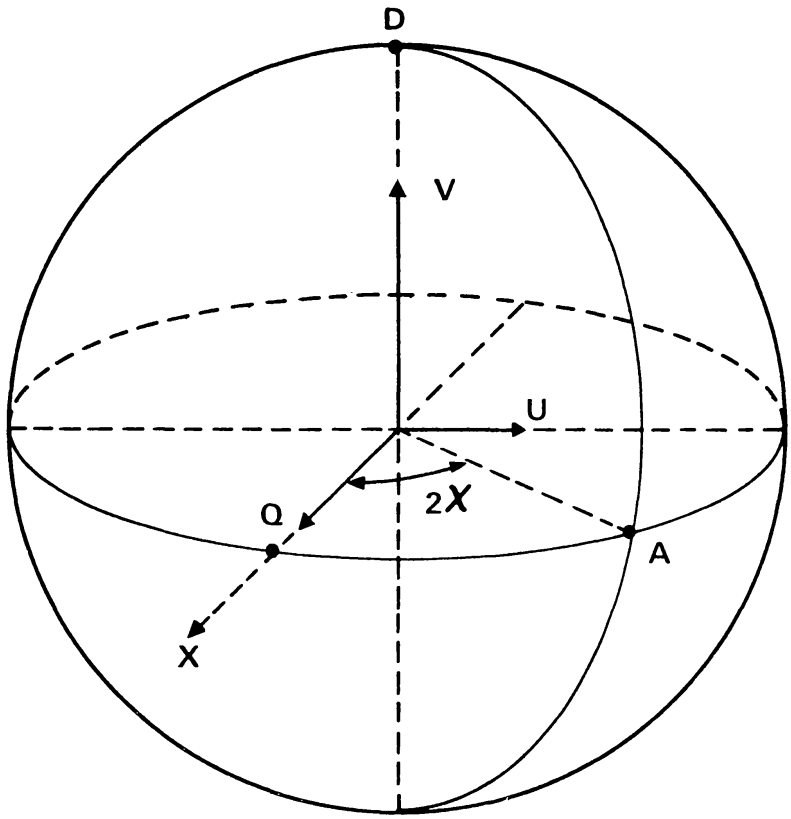

Fig. 2. The effect of two small rotations δ_A and δ_D of the Poincaré sphere around A and D is indicated here. The four Stokes parameters I, Q, U and V undergo the following changes:

$$\Delta I = 0$$
$$\Delta Q = -V \sin 2\chi \cdot \delta_A + U\delta_D$$
$$\Delta U = V \cos 2\chi \cdot \delta_A - U\delta_D$$
$$\Delta V = (Q \sin 2\chi - U \cos 2\chi)\, \delta_A .$$

4. Results

As an example, I have calculated the profile of the 5250.2 Å Fe line ($g=3$) which is frequently used in solar magnetographs. As input parameters I took: a) $N_{Fe}/N_H = 3.7 \times 10^{-6}$ (Goldberg *et al.*, 1959), b) $^{10}\log gf = -4.37$; c) the Bilberberg model solar atmosphere (Gingerich and De Jager, 1967); d) Doppler width $\Delta\lambda_D = 40$ mÅ, constant with depth; e) $a = 0.07$, constant with depth; f) no Doppler shift at any depth; g) scalar value of the field constant with depth; and h) $\cos\theta = 1.0$. None of these input parameters is restrictive; both $\Delta\lambda_D$ and a may, for example, vary with τ. In Figures 4 to 8 I show some line profiles for different conditions of the magnetic field. They were computed with the Sacramento Peak SDS Sigma 5 computer using a fourth-order Runge-Kutta integration technique. Integration was started at $\tau_B = 2.0$ with integration steps of 0.02 in τ. This resulted in accuracies of the Stokes parameters better than 1%. The figures show each of the Stokes parameters individually. The Q and U parameters may be combined to give the total amount of linearly-polarized light

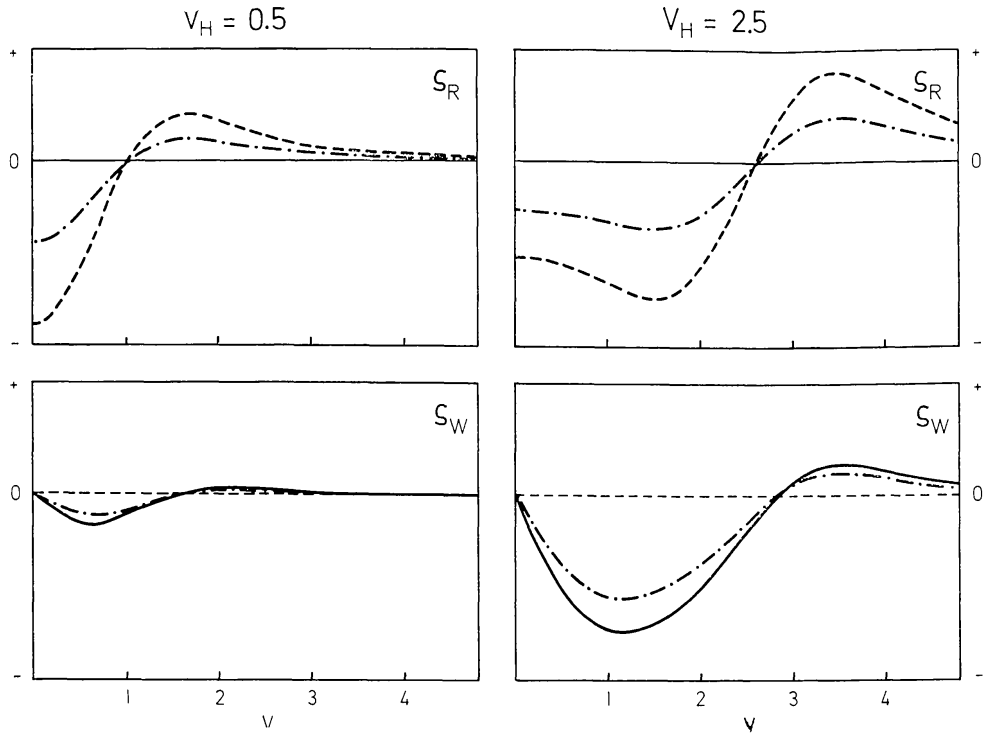

Fig. 3. Specific rotation ϱ_R and linear retardation ϱ_W for $v_H = 0.5$ (left) and $v_H = 2.5$ (right) and for $\gamma = 0°$ (-----), $\gamma = 90°$ (———), and $\gamma = 60°$ (–·–·). All retardations are on the same scale.

$\sqrt{(Q^2 + U^2)}$ and the azimuth of this polarization $\psi = 0.5$ arctan (U/Q). Only the red half of the line profiles are shown.

In understanding Figures 4 to 8 it is useful to draw the wavelength behavior of ϱ_W and ϱ_R. Figure 3 shows this for a Zeeman splitting $v_H = \Delta\lambda_H/\Delta\lambda_D = 0.5$ and 2.5. The amplitudes of ϱ_W and ϱ_R depend on γ and v_H.

4.1. Transverse field with variable azimuth

Figures 4 and 5 show the computation for $v_H = 2.5$ ($\approx$2500 G) and $v_H = 0.5$ ($\approx$500 G) respectively, with $\gamma = 90°$ and $\chi = \exp(-10\tau)$ radians for the original Unno Equations (1) and the modified Equations (16). Since the axis of retardation due to ϱ_W at small τ is not parallel to the polarization of the light originating at large τ, one obtains circularly-polarized light even for transverse fields. The shape of V is rather complex, but can easily be understood from the wavelength dependence of ϱ_W (Figure 3) and from the change of sign of Q and U. The V integrated over the line wing is not necessarily zero so that magnetographs which supposedly measure longitudinal fields (Evans, 1964; Beckers, 1968) could measure an apparent longitudinal field for a perfect transverse field.

The variation of χ with τ was taken so that the main variation occurred in the region where the line is formed. Because of the large increase of η_0 with decreasing τ ($\eta_0 = 0.1$, 4 and 21 at $\tau = 1.0$, 0.1 and 0.01, respectively) the 5250 line is formed at small τ. The changes in azimuth ψ are remarkably small considering the large vari-

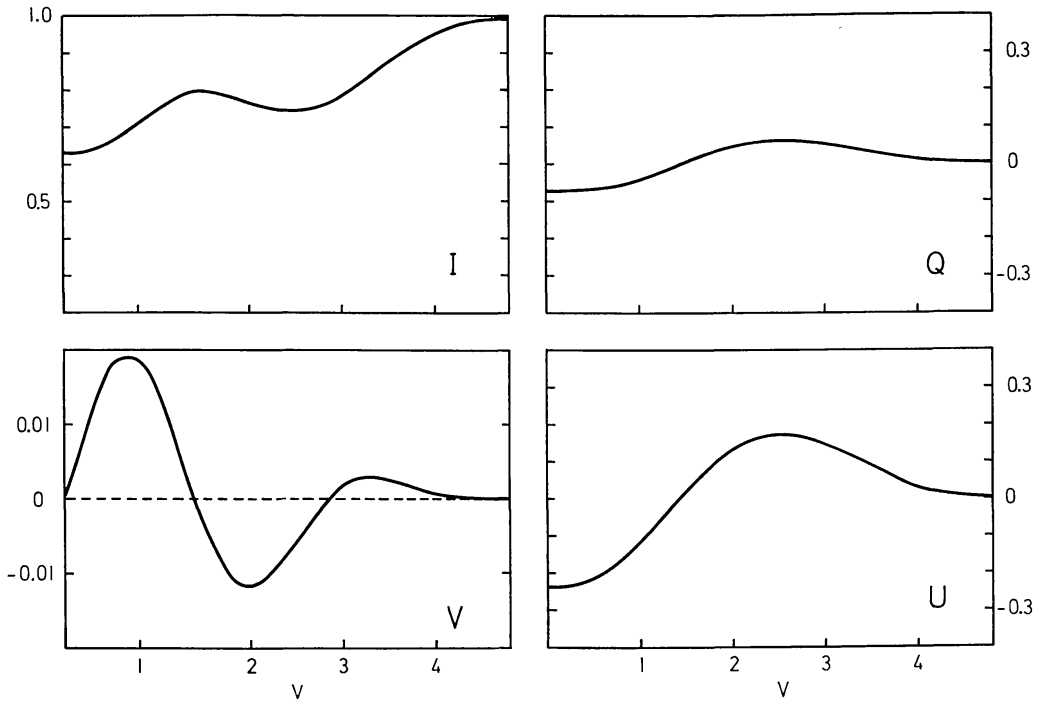

Fig. 4. Stokes parameters for a transverse field with a variable azimuth χ. Red half of the line only. The blue half is identical except for the reversal of V. $v_H = \Delta\lambda_H/\Delta\lambda_D = 2.5$, $\gamma = 90°$ and $\chi = \exp(-10\tau)$ radians. The dashed curves do not take into account magneto-optical effects. When the dashed and full-drawn curves virtually coincide, only the full-drawn curve is shown. Note that the curves have an unequal ordinate scale.

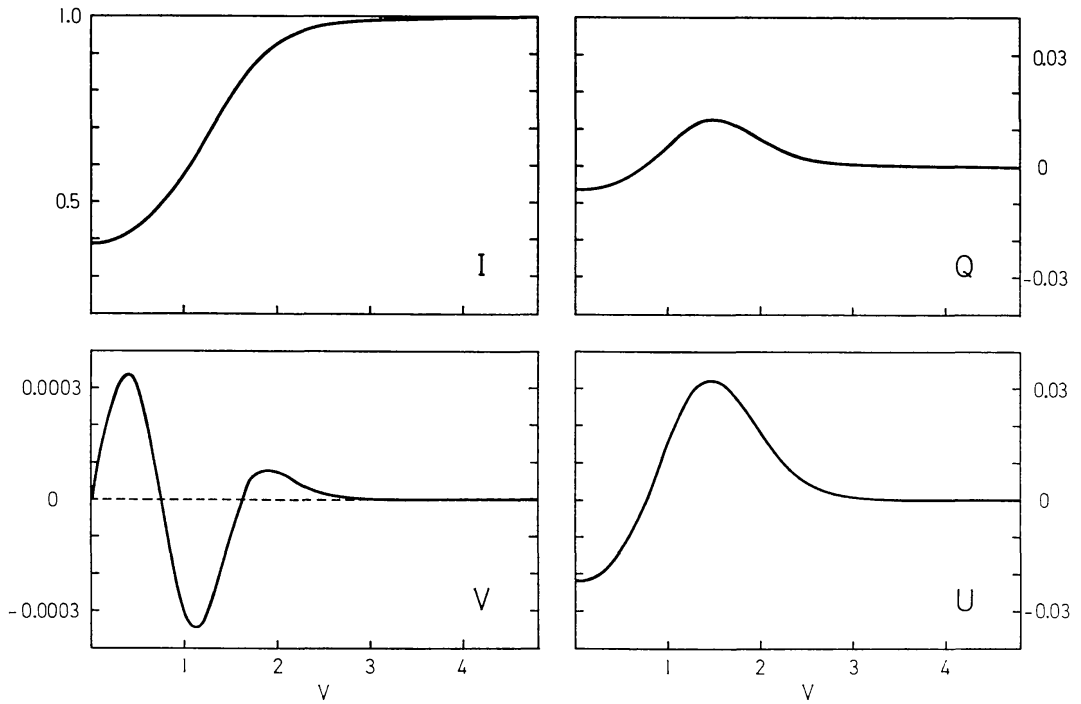

Fig. 5. As Figure 4, but with $v_H = 0.5$, $\gamma = 90°$, and $\chi = \exp(-10\tau)$ radians.

ation in χ. From line wing to line center these are $\approx 3°$. The direction of change is as one would expect: ψ is largest in the line center (36.8° or 0.64 radian at $v_H = 2.5$, and 37.1° or 0.65 radian at $v_H = 0.5$). Neglect of magneto-optical effects results in errors of ψ less than 0.4° and in $\sqrt{(Q^2 + U^2)}$ of less than 1%. The principal interest of the Voigt effect therefore lies in the generation of a non-zero V-Stokes parameter.

4.2. Field with variable γ but constant azimuth

Figures 6 and 7 illustrate the cases with $v_H = 2.5$ and 0.5 for $\gamma = \exp(-10\tau)$ radians and $\chi = 0$. Whereas in the $\gamma = 90°$ case the only magneto-optical effect was that of a linear retarder, one now has the combined effect of a rotator and a linear retarder. The optical axis of the latter is at $\chi = 0$. It can be seen from Figures 6 and 7 that the

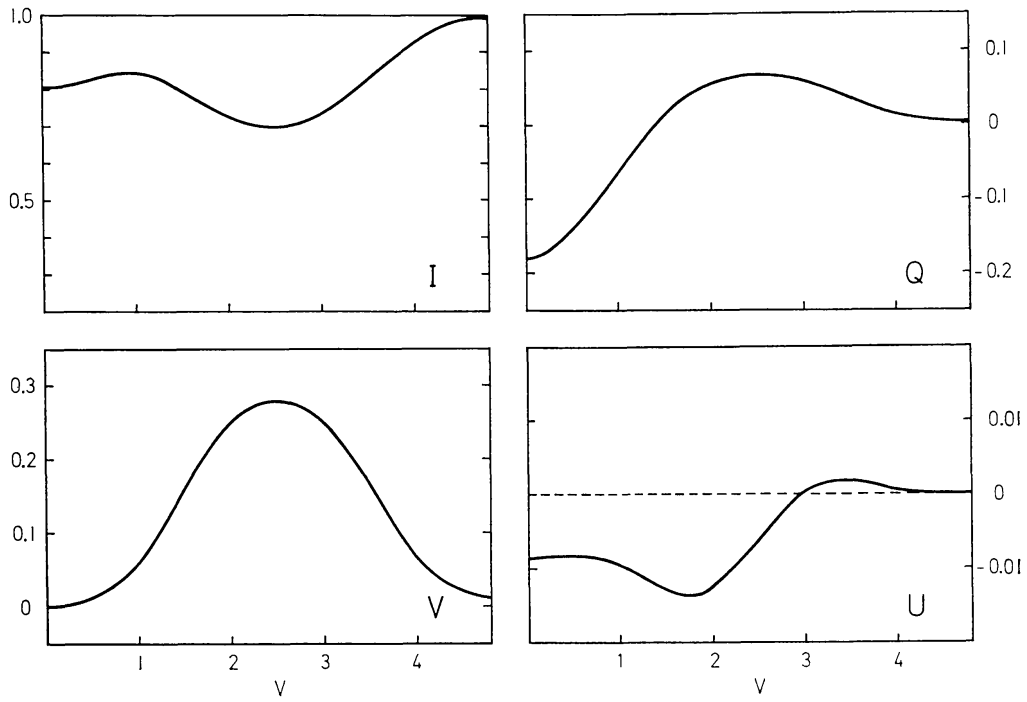

Fig. 6. As Figure 4, but with $v_H = 2.5$, $\gamma = \exp(-10\tau)$ radians, and $\chi = 0°$.

main effect of this is to make U non-zero. Both ϱ_R and ϱ_W contribute to the non-zero U by contributions from Q and V, respectively. The relatively large value for U, both at $v_H = 0.5$ and 2.5, results in very large variations of the azimuth ψ, changes up to 45° do actually occur, since at the v where $Q = 0$, the U does not vanish. In the interpretation of the measurements changes in ψ (Severny, 1964, 1965), one therefore has to take into account magneto-optical effects.

4.3. Other directions of the field

When both χ and γ vary with optical depth a mixture of the effects described in subsections 4.1 and 4.2 will occur. Of the very many varieties of field directions which one could imagine, I want to discuss here only one.

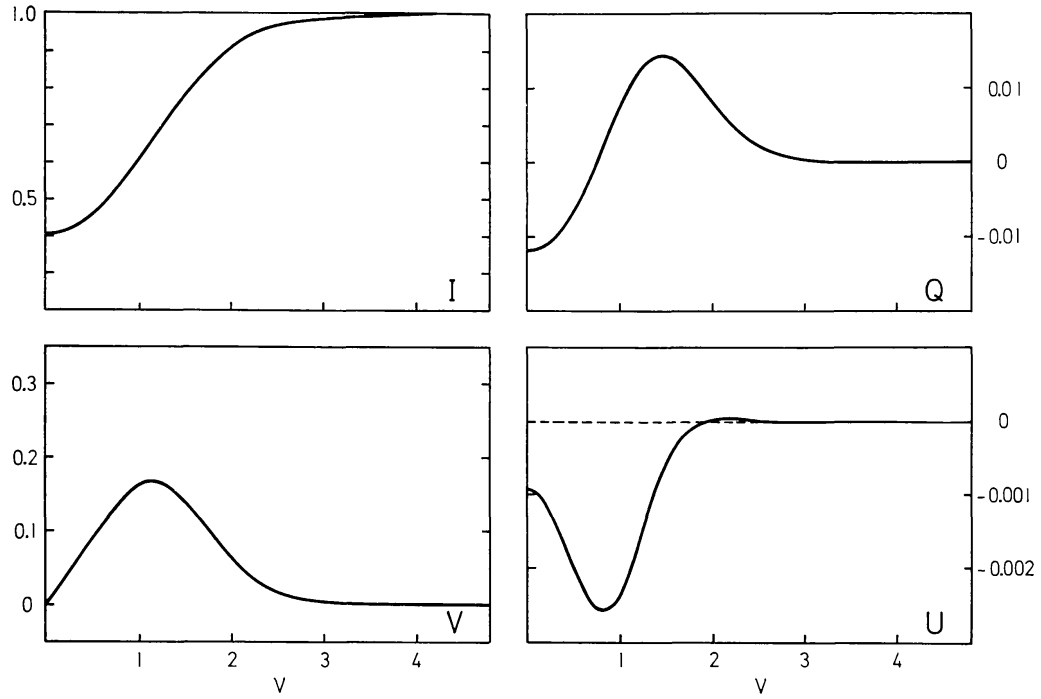

Fig. 7. As Figure 4, but with $v_H = 0.5$, $\gamma = \exp(-10\tau)$ radians, and $\chi = 0°$.

Beckers and Schröter (1968, 1969) discuss some accurate measurements of the V-Stokes parameter in sunspot umbrae. These measurements show this parameter to have an interesting behavior near the line center in the apparent π component. There the sign of V reverses and becomes opposite to that of the V of the σ component in

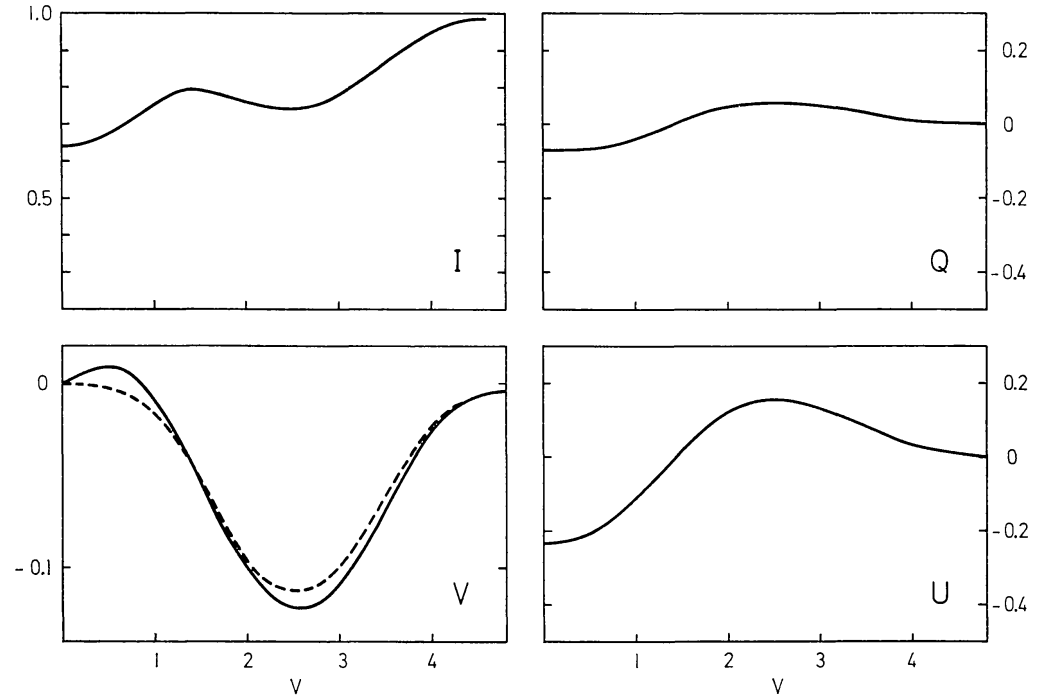

Fig. 8. As Figure 4, but with $v_H = 2.5$, $\gamma = 105°$, and $\chi = \exp(-10\tau)$ radians.

the same line wing. This effect was interpreted by assuming a two-component magnetic field structure (associated with the umbral dot structure). Such an inhomogeneous field would undoubtedly have large variations of the field direction over some 100 km associated with it so that the effects discussed in this paper will be present.

It is in fact possible to explain the observed V behavior by an azimuth variation of a partially longitudinal field (Rachkovsky, 1962a). The azimuth variation will give a variation of V as shown in Figure 4. The field being partially longitudinal will add to this a V similar to the one shown in Figure 6. In Figure 8 I show the Stokes parameters for such a case. I took $\gamma=105°$, $\chi=\exp(-10\tau)$ radians, and $v_H=2.5$. The V behaves exactly as expected.

It is interesting to note that the V reversal is only present for $\gamma<90°$ if χ increases with increasing τ and for $\gamma>90°$ if χ decreases with increasing τ. For $\gamma=75°$ and $\chi=\exp(-10\tau)$, for example, the main red wing V is positive as is the part of the Voigt-effect-related V that caused the reversal for $\gamma=105°$. If the behavior as observed for the V by Beckers and Schröter (1969) for one spot is universal and if it should be explained in the sense suggested above (which is unlikely), it would mean that all north polarities ($\gamma<90°$) must have an anticlockwise rotation of the field azimuth with increasing τ whereas south polarities ($\gamma>90°$) must have a clockwise rotation.

4.4. Magneto-optical effects with homogeneous fields

As Rachkovsky (1962b) pointed out, one has also to take into account magneto-optical effects when γ and χ are constant with depth for values of $\gamma\neq 0°$, 90° or 180° in case the Zeeman splitting is incomplete. As already seen in Section 3, one has no effects from the atmospheric birefringence in purely longitudinal and transverse homogeneous fields. Also, for complete splitting at any γ, the direction of retardation on the Poincaré sphere (Figure 1) coincides with the location of the polarization on the sphere. However, for incomplete splitting (e.g., $v_H=0.5$) this will not be the case so that the generalized Equations (16) will have to be used.

5. Conclusion

A direct numerical solution of Unno's equations proved quite simple although rather time-consuming. The numerical solution allows variation of all atmospheric conditions with optical depth. In case the magnetic field direction varies with depth or in case of a homogeneous field with $\gamma\neq 0°$, 90° or 180° one has to consider magneto-optical effects. The influence of these effects, however, is far less severe than Severny (1959) and Kai (1968) suggested. They are of the magnitude estimated by Rachkovsky (1962a, b). Errors in the estimates of the direction of the solar field may result if the magneto-optical effects are neglected. So one may, for example, observe an apparent longitudinal magnetic field with the nominally longitudinal magnetograph, even when the field is purely transverse, if its azimuth varies with height.

It would be very interesting to make a precise investigation of all Stokes parameters

within a sunspot in various lines. Such a study would show how severe magnetic field variations are in the formation of Zeeman-split lines. One would hope that such measurements would result in a model for the depth variation of **H**. However, we do not know whether an observed profile would necessarily have a unique $\mathbf{H}(\tau)$ relation associated with it.

References

Abramowitz, M. and Stegun, I. A.: 1964, *Handbook of Mathematical Functions*, (N.B.S. Applied Math. Series No. 55), Dover Publ., New York.
Aller, L. H.: 1963, *The Atmospheres of Sun and Stars*, Ronald Press, New York.
Beckers, J. M.: 1968, *Solar Phys.* **5**, 15.
Beckers, J. M. and Schröter, E. H.: 1968, *Solar Phys.* **4**, 303.
Beckers, J. M. and Schröter, E. H.: 1969, *Solar Phys.* **7**, 22.
Born, M.: 1965, *Optik*, 2nd. ed., Springer-Verlag, New York.
Evans, J. W.: 1964, *Rome Meeting on Solar Magnetic Fields*, p. 123.
Gingerich, O. and De Jager, C.: 1967, *Solar Phys.* **3**, 5.
Goldberg, L., Müller, E. A. and Aller, L. H.: 1960, *Astrophys. J. Suppl. Ser.* **45**, 1.
Harris, D. L.: 1948, *Astrophys. J.* **108**, 112.
Julius, W. H.: 1928, *Leerboek der Zonnephysica*, Noordhoff, Groningen.
Kai, K.: 1968, *Publ. Astron. Soc. Japan* **20**, 154.
Moe, O. K.: 1968, *Solar Phys.* **4**, 267.
Rachkovsky, D. N.: 1962a, *Izv. Krymsk. Astrofiz. Observ.* **27**, 148.
Rachkovsky, D. N.: 1962b, *Izv. Krymsk. Astrofiz. Observ.* **28**, 259.
Severny, A. B.: 1959, *Soviet Astron.* **3**, 214.
Severny, A. B.: 1964, *Izv. Krymsk. Astrofiz. Observ.* **31**, 126.
Severny, A. B.: 1965, *Izv. Krymsk. Astrofiz. Observ.* **33**, 3.
Unno, W.: 1956, *Publ. Astron. Soc. Japan* **8**, 108.